

Improvement in ion confinement time with multigrid configuration in an inertial electrostatic confinement fusion device

L. Saikia ¹, S. Adhikari ², S. R. Mohanty ^{1,3,*}, and D. Bhattacharjee ⁴

¹*Centre of Plasma Physics-Institute for Plasma Research, Sonapur, Kamrup 782402, India*

²*Institute for Energy Technology, Instituttveien 8, 2007 Kjeller, Norway*

³*Homi Bhabha National Institute, Anushaktinagar, Mumbai, Maharashtra, 400094, India*

⁴*Bhawanipur Anchalik College, Bhawanipur, Barpeta 781352, Assam, India*



(Received 14 February 2024; accepted 17 June 2024; published 15 July 2024)

Improvement in the functionality of an inertial electrostatic confinement fusion (IECF) device has been investigated through kinetic simulation. Previously, we achieved a neutron generation rate of 10^6 neutrons per second, but higher rates and better plasma confinement are necessary for broader applications. We compared a traditional single-grid IECF device with a triple-grid variant to evaluate the benefits of using multiple grids for ion confinement. Our computational models, using the 2D-3V XOOPIC code, suggest that the triple-grid device, with its optimized potentials, could significantly enhance ion confinement. The models show that the triple-grid design directs ion beams more effectively to the center, in contrast with the more scattered ion distribution in the single-grid design. This results in longer ion lifetimes in the triple-grid system due to its modified electrostatic fields. In the standard single-grid IECF device, the primary reasons for ion loss are chaotic ion trajectories and interactions with residual gases. By operating the triple-grid device under very low background gas pressure and with a focused field structure, we expect to achieve improved ion confinement.

DOI: [10.1103/PhysRevE.110.015203](https://doi.org/10.1103/PhysRevE.110.015203)

I. INTRODUCTION

While magnetic confinement remains the primary focus for fusion energy, there has been significant interest in exploring alternative confinement methods aimed at creating smaller and more cost-effective fusion reactors. These alternative reactor designs often involve the use of converging ion beams with recirculating ions. Examples of such designs include inertial electrostatic confinement fusion (IECF), multigrid IECF, and the concept of periodically oscillating plasma [1]. In these systems, both ions and electrons contribute to the electrostatic potential, which plays a crucial role in facilitating the fusion process. Within the core region, highly energetic ions come together, leading to the production of particles like neutrons, protons, and x rays [1–4]. The idea of IECF was proposed by both Farnsworth [5] and Lavrent'ev [1], and it was subsequently improved by Hirsch [1,6,7]. The IECF system can operate effectively when specific conditions related to pressure, cathode voltage, grid design, transparency, and the choice of fuel gases (including hydrogen, helium, tritium, and deuterium) are met.

Although explored for fusion power, Rider [2,8] and Nevins [9,10] highlight challenges in achieving net energy gain due to the non-Maxwellian energy distribution in IECF devices. The energy needed to sustain this distribution during the required time scale for substantial fusion reactions is believed to surpass the potential fusion power output. Nonetheless, IECF devices still draw interest, especially as

economical neutron sources for applications like neutron activation analysis [11–13], medical isotope generation [14,15], neutron radiography [16,17], contraband and explosives identification [18–20], and spacecraft propulsion [21]. The diverse applications of the IECF system necessitate boosting neutron production rates (NPRs) through higher ion density and ion energy. Furthermore, it requires maintaining a more stable and significantly confined plasma with longer confinement durations [22].

Authors of several studies have shown that the NPR is strongly influenced by factors such as input power, cathode shape, and cathode material. NPR improvement has been documented by changing the cathode grid material from stainless steel (SS) to graphite and titanium as well as altering the cathode shape from a standard spherical wire grid to a buckyball shape [3,23]. The gas pressure, cathode voltage, and cathode current cannot be adjusted independently when producing ions through glow or hot cathode discharge; these conditions are interrelated. However, it is possible to overcome glow discharge limitations by introducing an external grid system with a single grid cathode [24]. To generate abundant ion beams, it is necessary to reduce charge exchange collisions during ion confinement by lowering gas pressure, which in turn increases discharge cathode voltage to maintain a constant cathode current. This leads to higher-energy ion beams [1,24]. Multigrid IECF devices are effective in achieving this by reducing gas pressure, increasing ion beam energy, and extending confinement time compared with single-grid systems [25]. Ion grid impact can be minimized by using a large positive grid bias, resulting in primarily electron losses [2,26]. The results align with theoretical and experimental

*Contact author: smruti@cpiipr.res.in

findings from previous research, emphasizing that improved ion confinement and reactivity enhance the performance of the IECF device, making it a more efficient portable neutron source. Thorson *et al.* [27] used a triple-grid arrangement with a cusp magnetic configuration in a spherical IECF device to enhance ion flow convergence. However, the impact of the multigrid configuration on core size, virtual anode, ion core plasma density, and floating potential remains unexplored. Multigrid IECF systems shield and restore the asymmetry in electric fields produced by higher cathode voltage stalks, stabilizing ion trajectories and enabling ion recirculation. McGuire *et al.* [25] demonstrated improved ion lifetimes and synchronized behavior of ions in previous work. Additionally, multigrid systems efficiently reduce gas pressure and increase ion beam energy compared with single-grid systems, as verified by Dietrich *et al.* [28] using multiple independently biased concentric grids. It is anticipated that reducing the cathode voltage could decrease ion confinement time by $1/e$. Dietrich [21] comprehensively analyzed ion beam passes, ion loss mechanisms, and confinement time, both computationally and experimentally. Noborio *et al.* [29] proposed that applying a titanium (Ti) layer onto SUS-316L SS electrodes could enhance the NPR under conditions of low gas pressure and voltage. This proposition was subsequently experimentally confirmed by Bakr *et al.* [30]. Their findings indicated that the normalized NPR results from the use of Ti were $\sim 3\text{--}4$ times higher than those obtained with SS electrodes.

In this paper, we have reconfigured our standard single-grid IECF setup into a more complex triple-grid configuration by adding two extra external grids around the central cathode grid. The main goal is to evaluate the effectiveness of a single-grid vs a triple-grid IECF device, particularly in terms of the impact of the multigrid approach on ion confinement. Authors of previous studies have indicated ion density in the triple-grid setup is in similar order with the single-grid, especially at lower applied potentials [31]. Our computational analysis points to significant improvements in ion confinement with the triple-grid system, particularly when optimizing potential configurations. Operating this system under minimal gas pressure and with a concentrated field structure is anticipated to further enhance ion confinement. The formation of ion beam channels is primarily attributed to the hill-like potential structure near the central cathode grid. Section II delves into the experimental framework for the triple-grid IECF, covering specific experimental parameters. For simulating plasma particles in a two-dimensional (2D) cross-section of the IECF device, we utilize an open-source, object-oriented particle-in-cell (PIC) code known as XOOPIC. Section III thoroughly examines the theoretical basis of this simulation, focusing on the calculation of ion confinement times. The simulation outcomes demonstrated that appropriate external grid potentials lead to the formation of ion beam packets, contrasting with the even ion distribution in a single-grid setup. Furthermore, studies of potential profiles are conducted under various multigrid biasing conditions and compared with results from the conventional single-grid case. Notably, Sec. IV highlights that the extended ion confinement time in the triple-grid system will significantly boost the NPR. This paper concludes by outlining various potential strategies for further improving the performance and efficiency of the IECF device.

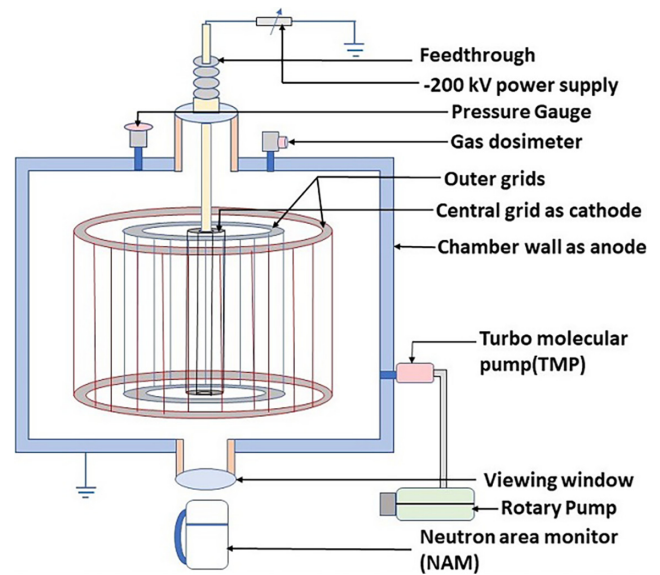


FIG. 1. Schematic diagram of triple-grid inertial electrostatic confinement fusion (IECF) configuration.

II. METHODS

A. Experimental setup

The IECF device, in its most fundamental configuration, comprises a central electrode positioned concentrically within a chamber which is a nearly transparent grid [31–36]. In this paper, we introduce two additional outer grids alongside the existing central cathode grid to investigate variations in ion flow dynamics. The chamber is built from 304 L SS, with dimensions of 50 cm in diameter and 30 cm in height, as shown in Fig. 1. It incorporates multiple ports facilitating various functions, including evacuation, gas injection, supplying voltage to the grids, and providing viewing windows. To produce a pristine plasma environment, it is essential to remove unwanted gases and impurities from the chamber. This is accomplished by achieving the desired low-pressure environment by employing a turbo molecular pump in conjunction with a rotary-vane pump. After evacuation, various gases such as hydrogen, deuterium, helium, tritium, and argon are introduced into the chamber as needed for our experiments. To power up the cathode grids, a significant negative voltage is supplied through a specialized high-voltage feedthrough. The central cathode grid is constructed with eight tungsten grid wires, providing a transparency of 90%, 3 cm in diameter. On the other hand, the intermediate and outer grids are crafted using SS wires, and they have diameters of 23 and 33 cm, respectively. Each of these external grids is equipped with 32 grid wires, and there are slight differences in their geometric transparencies due to their varying dimensions. Specifically, the intermediate grid has a transparency of 95%, whereas the outer grid has 96%. For the computational modeling of the device, a 2D-3V approach has been taken to reduce computational cost, keeping the physics intact. The cylindrical symmetry allowed us to reduce one dimension (height). However, considering the three dimensions (3D) of velocity allowed us to capture the complete picture of charged particle dynamics by means of the PIC approach. This approach is

TABLE I. Simulation parameters.

Parameters	Values
Grid size	360×360
System length	0.45 m
System width	0.45 m
Pulse duration	2000 μ s
Ion gun currents	50 μ A
Specific weight	5×10^5
Simulation time step	6×10^{-9} s
Geometry	Cartesian
Background gas	$^1\text{H}_2, ^2\text{H}_2$
Pressure	2.5×10^{-3} to 8×10^{-4} mbar

quite common among physicists and can be found in the literature across different fields of applications [37–40]. A more detailed discussion on the modeling approach is provided in the next section.

B. XOOPIC modeling for confinement estimations

We utilized the object-oriented PIC simulation tool developed by the Plasma Theory and Simulation Group at the University of California, Berkeley, known as XOOPIC [37,41] to advance our research in plasma physics modeling. This robust computational model facilitates the precise simulation of 2D phase space trajectories of electrons and ions within a designated plasma system, influenced by an electrostatic field. XOOPIC integrates a variety of collision models, including Monte Carlo collision techniques, and provides simulations of ion sources as well as detailed ionization models for ions and electrons applicable to various gaseous systems, including hydrogen, helium, and deuterium [21]. The capabilities of the model extend to fully relativistic computations for inertial particles and a Boltzmann framework for inertialess electrons [42]. Utilizing XOOPIC, we explored the detailed collision dynamics of charged particles, assessed ion confinement times, and mapped potential profiles across the plasma system. This in-depth use of XOOPIC has been instrumental in elucidating the complex physics underlying the operation of multigrad IECF devices, yielding insights comparable with those from experimental investigations.

For this modeling, we adopted specific simulation parameters outlined in Table I and designed a 2D cross-sectional geometry of the device, replicating the central and external cathode grids of the experimental setup, as shown in Fig. 2. The simulation domain included two electron guns and two ion guns positioned near opposite walls, each capable of emitting an equal flux of electrons and ions over a specified pulse duration. These electrons then interacted with the neutral gas, leading to the formation of positive ions through ionization collisions.

The dynamics of the electrons and ions were influenced by the potentials applied to the three grids within the simulation domain. We carefully selected the cell size to ensure it was consistently smaller than or equal to the Debye length under varying conditions. Throughout the simulation, we maintained the plasma density at $\sim 10^{13} \text{ m}^{-3}$. The time step size was determined by ensuring no particle moved more than one cell per step, thereby satisfying the Courant condition [43]. The time step size was calculated using the formula:

$$\Delta t = 0.3 \times \frac{d}{v}, \quad d = \frac{1}{\sqrt{\left(\frac{1}{dx}\right)^2 + \left(\frac{1}{dy}\right)^2}}, \quad (1)$$

where v is the drift velocity of the fastest particle (electron), and dx and dy are the cell sizes in the x and y directions, respectively. Upon substituting the appropriate values in Eq. (1), the time step is determined to be of the order of 10^{-10} s.

Poisson's equation was resolved using a multigrad Poisson solver that also incorporated the boundary conditions of the simulation [35]. This solver enhanced the speed of the solution and reduced the overall simulation time. Dirichlet boundary conditions were imposed by the solver along the computational grids at the boundaries of the simulation domain.

In this simulation, a significant number of macroparticles was used which, along with the relatively short domain length, helped minimize the statistical noise typical of PIC simulations. The simulation domain length and width are set to 0.45 m each to accommodate the external grids and charged particle injectors in the experimental setup. With a domain length of 0.45 m and a cell size (Δx) of 1.25×10^{-3} m (equivalent to the Debye length), the total number of grid cells is found to be 360 along each axis. Therefore, we specify a grid size 360×360 for the x and y simulation domains in Table I. The specific

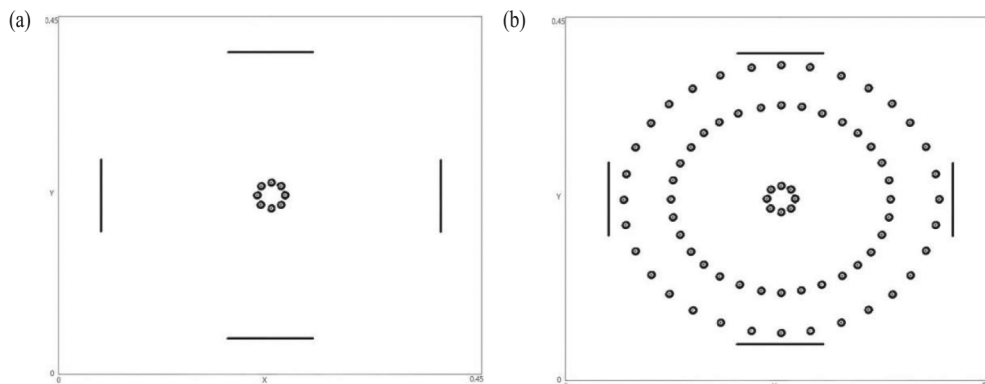


FIG. 2. Conceptual simulation domain for (a) single-grid and (b) triple-grid arrangement with electron and ion guns.

weight, defined as the ratio of the number of real particles to macroparticles, was set at 10^5 . This means that 0.1 million real particles are represented by 1 computational particle in our simulation. The XOOPIIC input file was constructed with all these parameters and conditions to facilitate the simulation. The output parameters of the simulation were saved in ASCII files, which were subsequently analyzed using various MATLAB scripts.

Prior to adopting the XOOPIIC code for our simulations of the IECF device, we evaluated several alternative simulation techniques. These methodologies provided valuable insights into the focusing characteristics and accurate field solutions for gridded fields with asymmetries [21]. Our initial research focused on the confinement properties of a standard IECF configuration featuring a single cathode grid. This exploratory phase revealed that employing a multigrid scheme effectively creates electrostatic lenses, which direct particles along radial trajectories.

For the simulations discussed, we set the central cathode potential at -5 kV, with the potentials of the external grids adjustable within a range from ± 100 to ± 800 V. Both hydrogen and deuterium were used as background gases, each demonstrating a similar mechanism for plasma confinement. This setup allowed us to closely replicate and analyze the dynamics within the IECF device, assessing the efficiency of different grid configurations in enhancing ion confinement.

III. RESULTS AND DISCUSSIONS

In this paper, a range of strategies is examined, including the operation of the device under reduced pressure conditions and the introduction of a multiple-grid configuration. We incorporate computational techniques to evaluate ion confinement time in a triple-grid configuration. Further, we also explore the effect of the external grids on potential profiles, and those are compared with the single-grid configuration.

A. Ion confinement time

The primary factor limiting the efficiency of IECF systems is the surpassingly momentary energy confinement time, specifically the short duration during which charged particles remain within the system. In standard IECF operating conditions, electrons emanate from the central cathode and get collected by the outer anode, while ions typically complete just a few orbits through the cathode before they are lost due to collisions with grid wires or charge-exchange reactions with background gases [25]. In a typical system, the likelihood of an ion being lost to a process other than fusion is roughly 100 000 times higher than being lost through a fusion reaction [21]. Therefore, enhancing the confinement of charged particles in IECF systems is a matter of paramount importance. McGuire [25] and Dietrich [21] worked on improvement in ion lifetime and synchronization behavior of multigrid configuration.

It is feasible to achieve substantial enhancements in ion confinement, even when utilizing electron and ion injectors that serve the dual role of being both sources and sinks for ions. When the simulated injectors are turned off, the number of ions in the system will decrease as ions are lost. The $1/e$

time of the decay curve can be compared with the expected confinement time based on the Hirsch [7] concept on the estimated average number of ions that pass through the central cathode grid before it is lost. To streamline the evaluation of the $1/e$ time, the ion signal is normalized to correspond to its state when the injection is turned off [21]. Although the maximum number of ions in the system may fluctuate depending on the strength of the source, the decay curve is solely determined by the ion sink. Consequently, the most accurate assessment of the actual confinement time in the device is obtained by comparing the $1/e$ times of the normalized decay curve. The ion confinement time and ion loss rate correlate with the following relation [21]:

$$1/e \text{ confinement time} \propto \frac{n_i}{\text{ion loss rate}}, \quad (2)$$

and

$$\text{ion loss rate} \propto n_i n_b \sigma v_i, \quad (3)$$

where

n_i	Ion density
n_b	Background gas density
σ	Charge exchange cross-section
v_i	Velocity of ion

Improved confinement is not observed in every multigrid situation [21]. In fact, ion confinement is anticipated to be affected by the specific grid potentials, as indicated by XOOPIIC modeling. Therefore, in this paper, simulations have been carried out by varying the external grid potentials and working gas pressures. In the single-grid configuration, ions experience a deviation from their intended radial paths, causing them to stray from the core of the device. Consequently, a broad distribution of ions throughout the domain is observed, as depicted in Fig. 3(a). In contrast, the triple-grid setup, with one of the external grids positively biased at $+500$ V, demonstrates the formation of tightly confined ion beams, as illustrated in Fig. 3(b). In this configuration, ion beams quickly form stable ion packets by small angle deviation, leading to collisions within the core where they intersect. The ion motion at the outer beam boundary results in low-energy Maxwellian distributions through local thermalization. Reacceleration by inner grids maintains monoenergetic ion beams, preserving average angular momentum and preventing energy loss. In the single-grid setup [Fig. 3(c)], an immediate drop in ion numbers is observed, signifying their rapid loss through interactions with the central grid wire via ion-ion collisions. Another loss mechanism involves unimpeded electron flow from the core to the chamber wall, happening within a $2001 \mu\text{s}$ time scale corresponding to a $2000 \mu\text{s}$ pulse duration, as depicted in the normalized decay curve [Fig. 3(e)]. Conversely, in the triple-grid arrangement, the electric fields near the cathode focus on ions rather than defocusing them, permitting ions to survive many oscillations. Ion trajectories are channeled into beams, preventing them from hitting the cathode. This is evidenced by the smooth ion decay profile in Fig. 3(d), indicating longer confinement. The $1/e$ times of the normalized decay curve yield an ion confinement time of $2675 \mu\text{s}$,

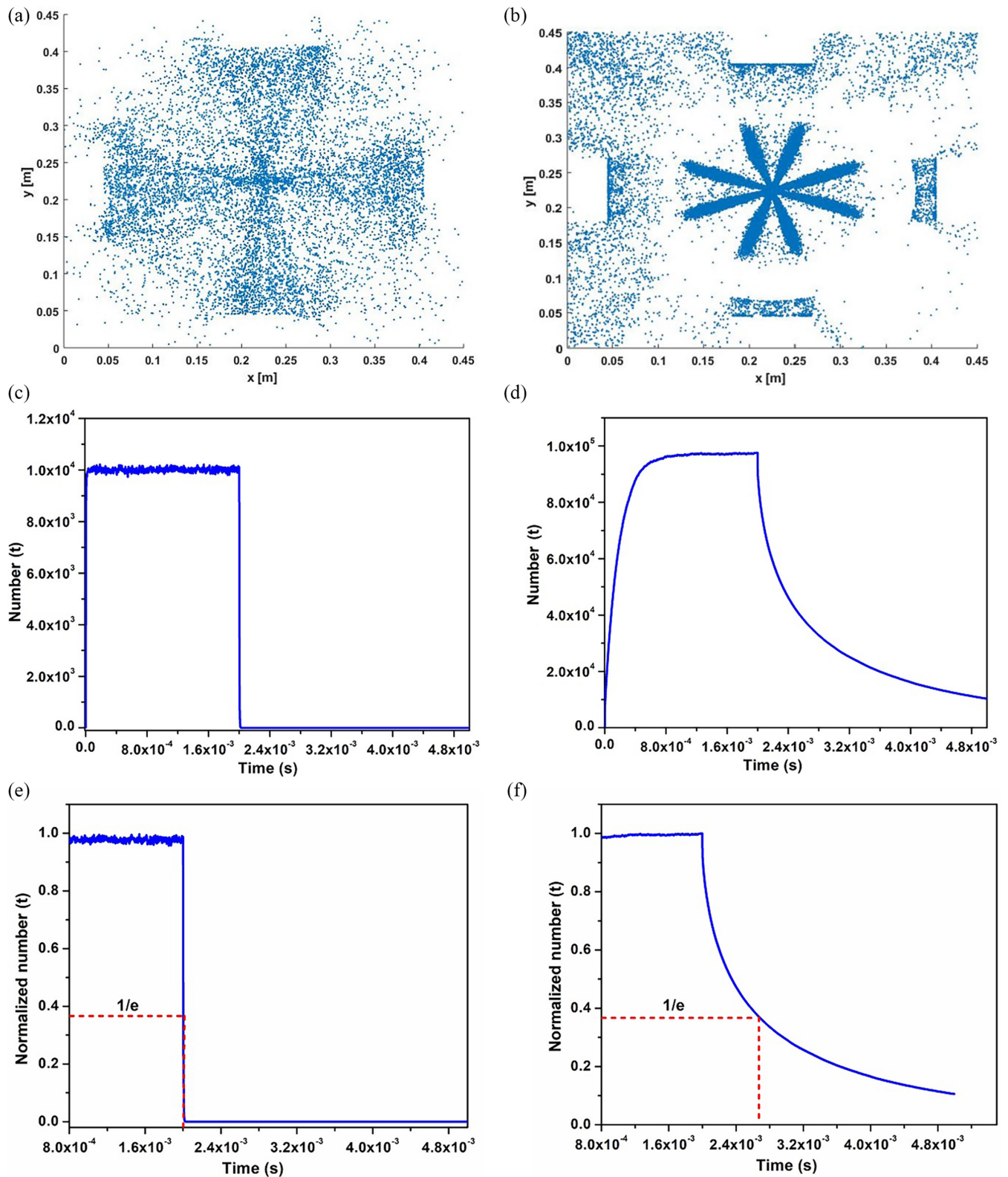


FIG. 3. (a) Ion phase space, (c) a typical plot depicting the number of macroparticles over time evolution, and (e) a normalized plot of the ion decay curve for the single-grid scenario at -5 kV on the central cathode grid. Additionally, (b) shows ion phase space, (d) presents a typical plot demonstrating the number of macroparticles with time evolution, and (f) exhibits a normalized plot of the ion decay curve for the triple-grid scenario at -5 kV on the cathode grid (central), $+500$ V on the intermediate grid, and the outer grid kept at a floating condition. These observations were made at a background gas pressure of 2.5×10^{-3} mbar.

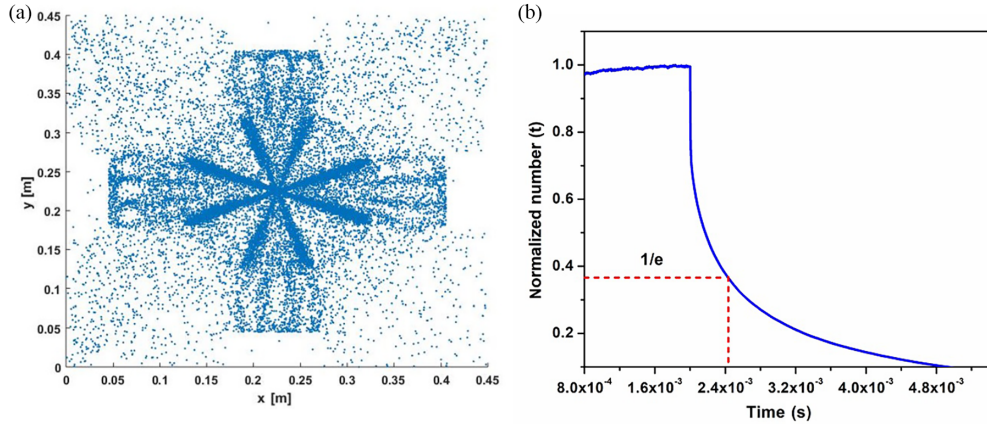


FIG. 4. (a) Ion phase space and (b) normalized plot of the ion decay curve for triple-grid scenario at -5 kV on central cathode grid and outer grids are kept at floating situation (background gas pressure 2.5×10^{-3} mbar).

as shown in Fig. 3(f). The comparative analysis results in a reduction of ion loss and enhancement in the duration of ion confinement within a triple-grid setting. An important finding from the examination of a triple-grid setup is that the presence of external grids alongside the central cathode grid led to prolonged confinement, even when the outer grids were floating, as indicated in Figs. 4(a) and 4(b). The floating outer grids extended the confinement time from $2001 \mu\text{s}$ [Fig. 3(e)] to $2428 \mu\text{s}$ [Fig. 4(b)]. This can be attributed to the acquisition of a negative potential by the external grids from the central cathode grid, subsequently altering the preexisting electric field and behaving like focusing lenses. Experimentally, it is verified that, when a voltage of -5 kV was applied to the central cathode grid, the intermediate and outer grids reached potentials of -125 and -30 V, respectively.

Evaluating the sensitivity of ion confinement to alterations in the potential setup is essential. Throughout the tests reported in this section, the central grid remained at a fixed -5 kV potential, while the potentials of the intermediate and outer grids are independently modified to investigate their influence on ion confinement duration. Initially, the primary emphasis is placed on studying how the ion confinement time responded to different potential levels for the intermediate grid, which included variations such as ± 100 , ± 300 , ± 500 , and ± 800 V, while the outer grid maintained a floating status. As illustrated in the comparative graph depicted in Fig. 5, an extension in ion confinement time is evident with a positive biasing of the intermediate grid, whereas a decrease in confinement is observed when the intermediate grid is biased negatively. This phenomenon can be attributed to the rapid occurrence of ion loss mechanisms during such specific potential scenarios. The phase space plot under negative intermediate grid biasing [Fig. 6] reveals the trajectory of ion beam lines traversing the intermediate grid, leading to ion loss through the impact on the grids. Although the simulation is designed to encompass a range of up to ± 800 V, experimental constraints have restricted us from applying a maximum of ± 500 V. Consequently, to further estimate the confinement time, we kept the biasing of the intermediate grid at $+500$ V, as it resulted in a confinement duration of $2675 \mu\text{s}$. Likewise, we plotted the variation in confinement time with different outer grid potentials while maintaining the intermediate grid at $+500$ V.

However, the use of an outer grid potential set at -500 V yields a reliable assessment of the confinement time when the intermediate grid potential was $+500$ V, as evidenced by Fig. 7. Nonetheless, the confinement time decreases with an increase in the positive potential. Although the combination of external grid potentials resulted in the maximum confinement of $2665 \mu\text{s}$ within this potential range, it is preferable to maintain the outer grid in a floating state, as this leads to a confinement duration of $2675 \mu\text{s}$ for ions.

Another significant mechanism for ion loss in an IECF device involves charge exchange with the background gas, as indicated in Eq. (3). Operating at high pressure increases the likelihood of charge exchange or ionization reactions occurring as compared with fusion. The ions generated by charge exchange collisions have insufficient energy to contribute to the reaction rate and are rapidly expelled by nonradial fields. Thus, it is imperative to run the system at lower pressure to optimize its performance. A shift in the optimal operat-

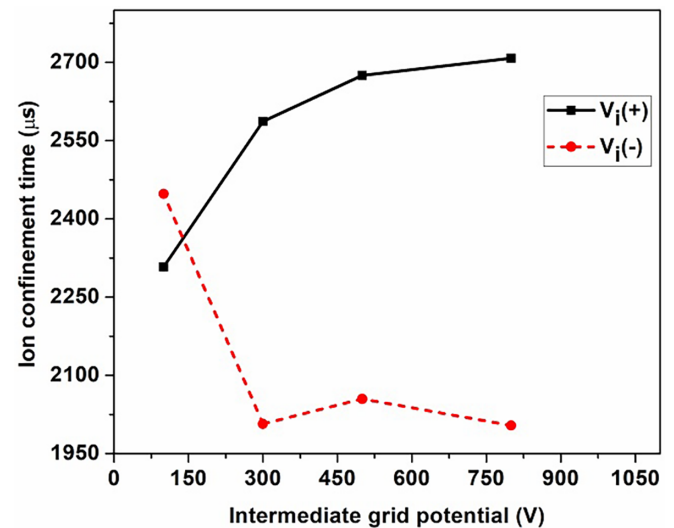


FIG. 5. Variation of ion confinement time for both positive and negative intermediate grid potentials keeping the outer grid at floating condition and the central cathode at -5 kV (background gas pressure 2.5×10^{-3} mbar).

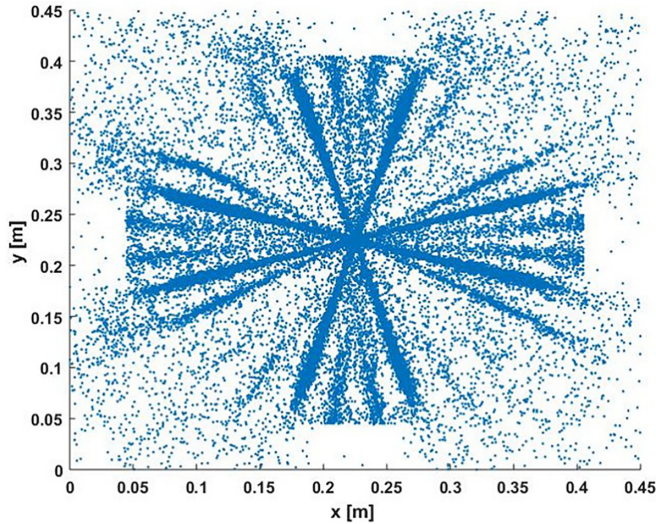


FIG. 6. Ion phase space plot for triple-grid scenario at -5 kV on central cathode, -500 V on intermediate and outer grid is kept at floating situation (background gas pressure 2.5×10^{-3} mbar).

ing range of the system toward lower pressures was made possible by our earlier study on the triple-grid arrangement [31]. Consequently, simulations are conducted to estimate ion confinement time while considering the impact of varying background gas pressure. In the triple-grid configuration, the grid potentials were set at -5 kV on the central cathode, $+500$ V on the intermediate grid, and -500 V on the outer grid. The flattening of trends at lower pressure suggests that the ion lifetime is primarily limited by a mechanism other than charge exchange, such as the direct impact of primary ions on the grid. As anticipated, the $1/e$ confinement time is inversely proportional to pressure in the case of the triple-grid configuration, as illustrated in Fig. 8. In contrast, under the investigated operating regimes, the $1/e$ confinement time for

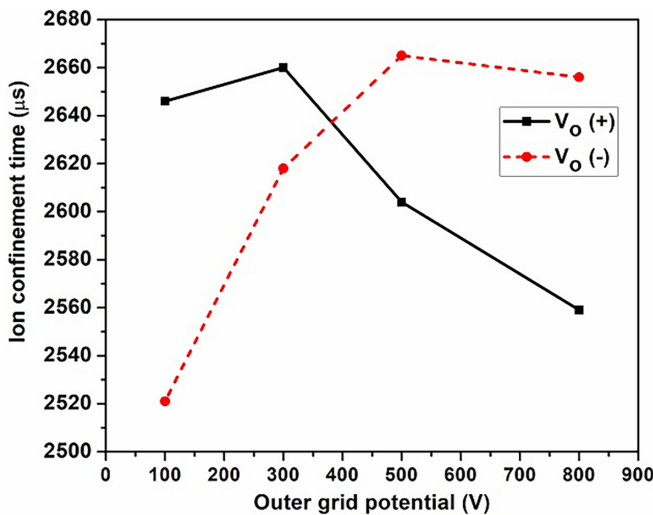


FIG. 7. Variation of ion confinement time for both positive and negative potentials of the outer grid. The potential of the intermediate and the central cathode grids are fixed at $+500$ V and -5 kV, respectively (background gas pressure 2.5×10^{-3} mbar).

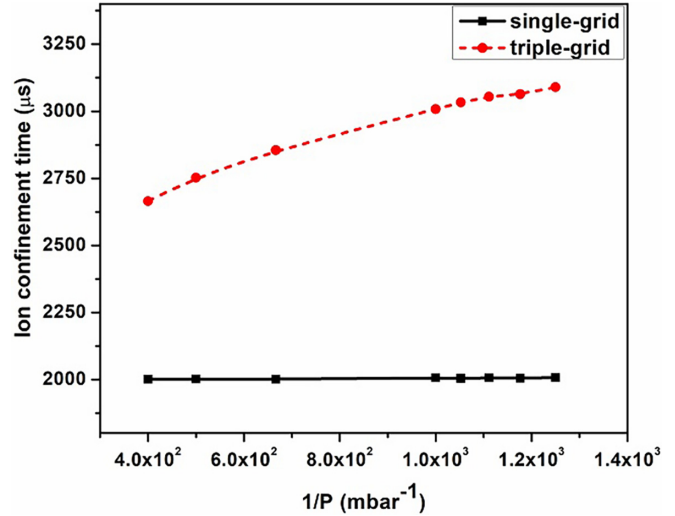


FIG. 8. Variation of ion confinement time with background gas pressure for single- and triple-grid configurations at -5 kV on the central grid, $+500$ V on the intermediate, and -500 V on the outer grid.

the single-grid arrangement shows a general insensitivity to pressure. The dotted red line in Fig. 8 distinctly illustrates an enhancement in ion confinement, increasing from 2665 to 3090 μ s, as the background gas pressure is reduced from 2.5×10^{-3} to 8×10^{-4} mbar.

B. Potential profile study

The formation of multiple potential wells within the central cathode grid establishes the essential confinement mechanism, rendering the IECF device an efficient fusion reactor. In our earlier experimental work [31], we already discussed the potential profiles for multigrid configuration and compared the results with a single-grid one. Initially, a potential study in this triple-grid configuration carried out our interest toward the formation of multiple potential wells, but later, observation of the potential profile strongly showed its importance in potential well depth reduction and the formation of hill-like structures outside the central cathode. This empirical observation is further validated through XOOPIC simulations, where the potential of the central cathode is maintained at -5 kV, while the potentials of the external grids are altered. A 3D surface plot is employed to illustrate the potential distribution within the IECF device and showcase the modifications in the potential profile stemming from the introduction of triple-grid configurations compared with a traditional system. In the instance of a single grid [see Fig. 9(a)], a well depth of roughly -5 kV is observable, extending extensively across the domain (~ 45 cm), aligning with the applied cathode potential of -5 kV. On the other hand, a more confined well (~ 16 cm) extending up to the diameter of the intermediate grid is noted in the triple-grid setup, where there is a decrease in well depth at -5 kV on the central grid and $+500$ V on the intermediate grid, as depicted in Fig. 9(b). The application of a positive potential on the external grid leads to the creation of potential hills and is accountable for the development of constrained, thick ion beam channels, as illustrated in Fig. 3(b). In contrast,

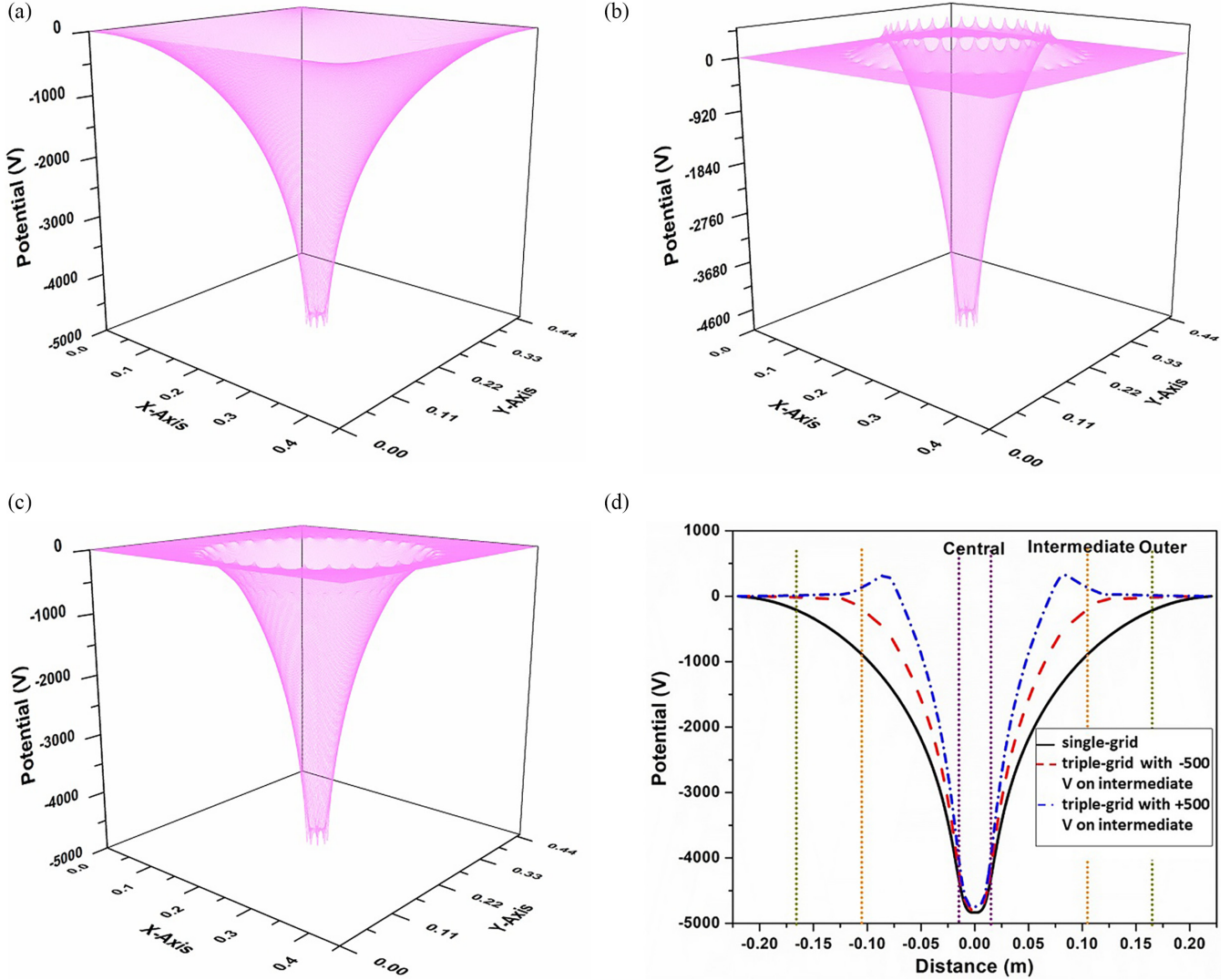


FIG. 9. Simulated three-dimensional (3D) surface potential profiles at -5 kV central grid voltage for (a) single-grid case, (b) triple-grid with $+500$ V on intermediate grid, and (c) triple-grid with -500 V on intermediate grid, where outer grid is kept at floating situation. The x - y potential profile with different grid biasing conditions is shown in (d).

a negative potential on the external grid [Fig. 9(c)] results in a considerably broader potential well (~ 22 cm) than the positive scenario, resulting in a mild hill-like configuration. Consequently, we observed widely dispersed thin ion beam channels in the case of negative applied voltage on the external grid, as seen in Fig. 6. The common potential profiles across the simulation domain distinctly reveal the appearance of a narrower potential well in the triple-grid configuration than the single-grid setup, along with the formation of potential hills as shown in Fig. 9(d). The more constricted potential well effectively confines ions and limits their loss to the surroundings. This observation provides evidence of the existence of ion beam channels, indicating an enhancement in ion confinement time within the triple-grid setup, particularly when there is a positive potential applied to the external grid.

Numerical simulations use physical principles to create an accurate model, enabling a detailed analysis of a plasma device on a smaller scale. By simulating numerous interacting macroparticles within a predefined shape, plasma properties can be efficiently explored throughout the device. Never-

theless, these simulations are restricted by the precision in representing microscopic phenomena and field solutions. The present serial code runs on a single CPU and has a limited computational grid resolution, making it insufficient for scenarios with greater cathode voltages. In that context, we look forward to exploring computational tools to overcome the stated problems.

IV. SUMMARY AND FUTURE SCOPE

The performance of a triple-gridded IECF configuration in terms of ion confinement mechanism has been studied with XOOPIC simulation. The outcomes of our computational analyses represent a significant enhancement in ion confinement achieved through the implementation of a triple-grid system as compared with the traditional single-grid system. Through rigorous simulations using the XOOPIC code, we have quantified the $1/e$ confinement duration under various configurations of grid potentials and operating gas pressures. These simulations reveal that the triple-grid configuration not

only exhibits a dependence on pressure for its confinement efficiency but also highlights the crucial role of external grids in extending ion lifetimes, even when these grids are not actively powered. This finding also underscores the potential of this configuration to operate optimally at lower pressures, aligning with previous experimental observations and highlighting its suitability for applications requiring prolonged ion confinement. The simulated 3D surface potential plots disclose a notably modified and tightly confined potential well in triple-grid setups, contrasting with the single-grid configuration. The appearance of potential hills initiates a recirculation phenomenon among ions, resulting in the formation of strongly confined channelized ion beams. This repetitive recirculation reduces ion loss and prolongs ion confinement time within the triple-grid setup.

In our future work, we plan to focus on two main areas: XOOPIC simulations to be accomplished by considering

the electromagnetic effects for a better understanding of ion confinement mechanisms and, by performing experiments, to measure how electromagnetic effects can improve NPR. The enhancement of NPR expands the applicability of the triple-grid IECF system across various practical domains.

ACKNOWLEDGMENTS

The authors express gratitude to the Director of the Institute for Plasma Research, Gandhinagar, India, and the Centre Director of the Centre of Plasma Physics Institute for Plasma Research, Sonapur, India, for their support in conducting this study. The authors recognize the valuable discussions with Dr. Sanjib Kalita, Dr. Rakesh Moulick, and Dr. Gunjan Sharma.

-
- [1] G. H. Miley and S. K. Murali, *Inertial Electrostatic Confinement (IEC) Fusion* (Springer, New York, 2014).
- [2] T. H. Rider, A general critique of inertial-electrostatic confinement fusion systems, *Phys. Plasmas* **2**, 1853 (1995).
- [3] M. Bakr, J. P. Wulfschlegel, K. Mukai, K. Masuda, M. Tajmar, and S. Konishi, Evaluation of 3D printed buckyball-shaped cathodes of titanium and stainless-steel for IEC fusion system, *Phys. Plasmas* **28**, 012706 (2021).
- [4] D. Tiedemann, P. Hofmann, J. Emmerlich, Y. A. Chan, S. Ulrich, G. Herdrich, and M. Muller, Cylindrical inertial electrostatic confinement plasma source for surface treatment, *Vacuum* **193**, 110502 (2021).
- [5] P. T. Farnsworth, Electric discharge device for producing interactions between nuclei, U.S. patent 3,258,402 (1966).
- [6] T. J. Dolan, Magnetic electrostatic plasma confinement, *Plasma Phys. Control. Fusion* **36**, 1539 (1994).
- [7] R. L. Hirsch, Experimental studies of a deep, negative, electrostatic potential well in spherical geometry, *Phys. Fluids* **11**, 2486 (1968).
- [8] T. H. Rider, Fundamental limitations on plasma fusion systems not in thermodynamic equilibrium, *Phys. Plasmas* **4**, 1039 (1997).
- [9] W. M. Nevins, Can inertial electrostatic confinement work beyond the ion-ion collisional time scale? *Phys. Plasmas* **2**, 3804 (1995).
- [10] W. M. Nevins, A review of confinement requirements for advanced fuels, *J. Fusion Energy* **17**, 25 (1998).
- [11] D. L. Bleuel, C. B. Yeamans, L. A. Bernstein, R. M. Bionta, J. A. Caggiano, D. T. Casey, G. W. Cooper, O. B. Drury, J. A. Frenje, C. A. Hagmann *et al.*, Neutron activation diagnostics at the National Ignition Facility (invited), *Rev. Sci. Instrum.* **83**, 10D313 (2012).
- [12] G. H. Miley, H. Momota, H. Leon, B. Ulmen, G. Amadio, A. Khan, G. Chen, W. Matisiak, A. Azeem, and P. Keutelian, Cylindrical IEC fusion neutron source for broad area NAA, *J. Eng. Gas Turb. Power* **133**, 124502 (2011).
- [13] J. C. Laul, Neutron activation analysis of geological materials, *At. Energy Rev.* **17**, 603 (1979).
- [14] B. B. Cipiti and G. L. Kulcinski, Embedded D-³He fusion reactions and medical isotope production in an inertial electrostatic confinement device, *Fusion Sci. Technol.* **44**, 534 (2003).
- [15] B. B. Cipiti, The fusion of advanced fuels to produce medical isotopes using inertial electrostatic confinement, Ph.D. thesis, University of Wisconsin, Madison, 2004.
- [16] M. Strobl, I. Manke, N. Kardjilov, A. Hilger, M. Dawson, and J. Banhart, Advances in neutron radiography and tomography, *J. Phys. D* **42**, 243001 (2009).
- [17] N. Kardjilov, I. Manke, A. Hilger, M. Strobl, and J. Banhart, Neutron imaging in materials science, *Mater. Today* **14**, 248 (2011).
- [18] A. Bueffer, Contraband detection with fast neutrons, *Radiat. Phys. Chem.* **71**, 853 (2004).
- [19] K. Yoshikawa, K. Masuda, T. Takamatsu, E. Hotta, K. Yamauchi, S. Shiroya, T. Misawa, Y. Takahashi, M. Ohnishi, and H. Osawa, Research and development on humanitarian landmine detection system by use of a compact D-D fusion neutron source, *Fusion Sci. Technol.* **52**, 1092 (2007).
- [20] N. Elsheikh, G. Viesti, I. ElAgib, and F. Habbani, On the use of a (²⁵²Cf-³He) assembly for landmine detection by the neutron back-scattering method, *Appl. Radiat. Isot.* **70**, 643 (2012).
- [21] C. C. Dietrich, Improving particle confinement in inertial electrostatic fusion for spacecraft power and propulsion, Ph.D. thesis, Massachusetts Institute of Technology, Cambridge, 2007.
- [22] K. Noborio, Y. Yamamoto, Y. Ueno, and S. Konishi, Confinement of ions in an inertial electrostatic confinement fusion (IECF) device and its influence on neutron production rate, *Fusion Eng. Des.* **81**, 1701 (2006).
- [23] R. Bowden-Reid and J. Khachan, An inertial electrostatic confinement fusion system based on graphite, *Phys. Plasmas* **28**, 042703 (2021).
- [24] K. Masuda, K. Taruya, T. Koyama, H. Hashimoto, K. Yoshikawa, H. Toku, Y. Yamamoto, M. Ohnishi, H. Horiike, and N. Inoue, Performance characteristics of an inertial electrostatic confinement fusion device with a triple-grid system, *Fusion Sci. Technol.* **39**, 1202 (2001).

- [25] T. J. McGuire, Improved lifetimes and synchronization behavior in multi-grid inertial electrostatic confinement fusion devices, Ph.D. thesis, Massachusetts Institute of Technology, Cambridge, 2007.
- [26] R. Radel and G. Kulcinski, Effects of high temperature pulsed helium implantation on tungsten surface morphology, *Fusion Sci. Technol.* **52**, 544 (2007).
- [27] T. A. Thorson, R. D. Durst, R. J. Fonck, and L. P. Wainwright, Convergence, electrostatic potential, and density measurements in a spherically convergent ion focus, *Phys. Plasmas* **4**, 4 (1997).
- [28] C. C. Dietrich, L. J. Eurice, and R. J. Sedwick, Experimental verification of enhanced confinement in a multi-grid IEC device, in *44th AIAA/ASME/SAE/ASEE Joint Propulsion Conference & Exhibit* (American Institute of Aeronautics and Astronautics, Hartford, 2008).
- [29] K. Noborio, Y. Yamamoto, and S. Konishi, Neutron production rate of inertial electrostatic confinement fusion device with fusion reaction on surface of electrodes, *Fusion Sci. Technol.* **52**, 1105 (2007).
- [30] M. Bakr, K. Masuda, and M. Yoshida, Improvement of the neutron production rate of IEC fusion device by the fusion reaction on the inner surface of the IEC chamber, *Fusion Sci. Technol.* **75**, 479 (2019).
- [31] L. Saikia, D. Bhattacharjee, S. R. Mohanty, and S. Adhikari, Studies on ion flow dynamics in a disk-shaped inertial electrostatic confinement fusion device under the influence of a triple grid arrangement, *Phys. Plasmas* **30**, 022110 (2023).
- [32] N. Buzarbaruah, N. J. Dutta, J. K. Bhardwaz, and S. R. Mohanty, Design of a linear neutron source, *Fusion Eng. Des.* **90**, 97 (2015).
- [33] N. Buzarbaruah, N. Dutta, D. Borgohain, S. R. Mohanty, and H. Bailung, Study on discharge plasma in a cylindrical inertial electrostatic confinement fusion device, *Phys. Lett. A* **381**, 2391 (2017).
- [34] N. Buzarbaruah, S. R. Mohanty, and E. Hotta, A study on neutron emission from a cylindrical inertial electrostatic confinement device, *Nucl. Instrum. Methodes Phys. Res. A* **911**, 66 (2018).
- [35] D. Bhattacharjee, N. Buzarbaruah, S. R. Mohanty, and S. Adhikari, Kinetic characteristics of ions in an inertial electrostatic confinement device, *Phys. Rev. E* **102**, 063205 (2020).
- [36] D. Bhattacharjee, N. Buzarbaruah, and S. R. Mohanty, Neutron and x-ray emission from a cylindrical inertial electrostatic confinement fusion device and their applications, *J. Appl. Phys.* **130**, 053302 (2021).
- [37] J. P. Verboncoeur, A. B. Langdon, and N. T. Gladd, An object-oriented electromagnetic PIC code, *Comput. Phys. Commun.* **87**, 199 (1995).
- [38] L. Wang, P. Hartmann, Z. Donko, Y. H. Song, and J. Schulze, 2D Particle-in-cell simulations of charged particle dynamics in geometrically asymmetric low pressure capacitive RF plasmas, *Plasma Sources Sci. Technol.* **30**, 085011 (2021).
- [39] J. Bai, Y. Cao, X. He, and E. Peng, An implicit particle-in-cell model based on anisotropic immersed-finite-element method, *Comput. Phys. Commun.* **261**, 107655 (2021).
- [40] H. Shah, S. Kamaria, R. Markandeya, M. Shah, and B. Chaudhury, A novel implementation of 2D3V particle-in-cell (PIC) algorithm for Kepler GPU architecture, *IEEE 24th International Conference on High Performance Computing (HiPC)* (Jaipur, India, 2017).
- [41] C. K. Birdsall and A. B. Langdon, *Plasma Physics via Computer Simulation* (CRC Press, Boca Raton, 2017).
- [42] D. L. Bruhwiler, R. E. Giacone, J. R. Cary, J. P. Verboncoeur, P. Mardahl, E. Esarey, W. P. Leemans, and B. A. Shadwick, Particle-in-cell simulations of plasma accelerators and electron-neutral collisions, *Phys. Rev. ST Accel. Beams* **4**, 101302 (2001).
- [43] C. De Moura, C. Kubrusly, and S. Carlos, *The Courant-Friedrichs-Lewy (CFL) Condition: 80 Years After its Discovery* (Springer, New York, 2013).